Complex Bifurcation Phenomena in a Tunnel Diode Model

Yu-Sheng Huang

Advisor: S.W.Teitsworth

April 2015

1 Abstract

Tunnel Diodes are semiconductor devices that have many uses in physics and other fields. In this thesis, we study the effect of negative differential conductance in the current-voltage(IV) characteristic region of the tunnel diode and study the resulting bifurcation phenomenon. We first study the 3D model that has been physically studied by Steven Jones. We are able to successfully construct the circuit model with nonlinear equations, characterize the bifurcation phenomena by constructing a phase diagram of the system and discovering evidence of the codimension 2 bifurcation phenomenon.

We then proceed to simplify the system by replacing the complicated form of the I-V characteristic with a cubic form. Non-dimensionalization of the

dynamical system is also conducted to study the system more carefully. Furthermore, we reduce the system to a 2D system. With these simplifications we are able to mathematically derive the bifurcation boundary of the system and determine the conditions for different bifurcations to occur. We are able to classify the conditions for the codimension 2 bifurcation to appear.

We are able to carry out simulations of the system and visualize the behavior of all these bifurcation phenomena. These numerical simulations identify and classify different bifurcations as well as unfold the bifurcation phenomena.

2 Introduction

Tunnel Diodes are semiconductor devices functionally similar to ordinary diodes. They have heavily doped p-n junctions with a narrow gap around 10-100 nm between the two region. This narrow gap allows quantum tunneling effects of electrons in the low voltage regions. At higher forward bias voltages, the behavior of tunnel diodes is similar to that of a normal diode.

The most important characteristic of a tunnel diode is the negative slope region in its I-V characteristic curve, known as negative differential conductance (NDC) [1]. In a conventional diode, conduction takes place while the p–n junction is forward biased and blocks current flow when the junction is reverse biased. This occurs up to a point known as the "reverse breakdown voltage" when conduction begins. In the tunnel diode, however, the dopant

concentrations in the p and n layers are increased to the point that the reverse breakdown voltage becomes zero and the diode conducts in the reverse direction. When forward-biased, quantum tunnelling occurs which gives rise to a region with an increase in forward voltage accompanied by a decrease in forward current[1].

Due to this negative region on the I-V curve, tunnel diodes are often used as oscillators and high-frequency threshold devices. Applications include local oscillators for UHF television tuners, trigger circuits in oscilloscopes, high-speed counter circuits, and very fast-rise time pulse generator circuits.[5]

This paper aims to study and characterize various behaviors in the tunnel diode system. We will be looking at full circuit system trying to unfold the bifurcations. We will also be approximating the tunnel diode system by using the cubic form approximation based on an experimental setup. This will enable us to further analyze the system using simulations as well as mathematical derivations. With the help of MATLAB and Mathmetica, we are able to study the stability of each fixed point as well as observe the interesting behavior of a possible codimension two bifurcation when a Hopf bifurcation intersects with a saddle node bifurcation. we are able to verify the result with mathematical derivation.

3 The 3D Tunnel Diode System

The equation that accurately describes the current-voltage (I-V) characteristic of the tunnel diode[2] is given here:

$$f(v_d) = i_1 \cdot \tanh(v_d/v_1) \cdot (C + e^{-K_1(v_d - v_2)^2}) + i_2 \cdot (e^{(v_d/v_3)} - 1) \qquad (1)$$

We are going to call this the complicated form for the I-V characteristic in comparison to other alternatives shown later in the paper. We can see in Figure 1 that the I-V characteristic curve shows a negative slope in the low voltage region as expected.

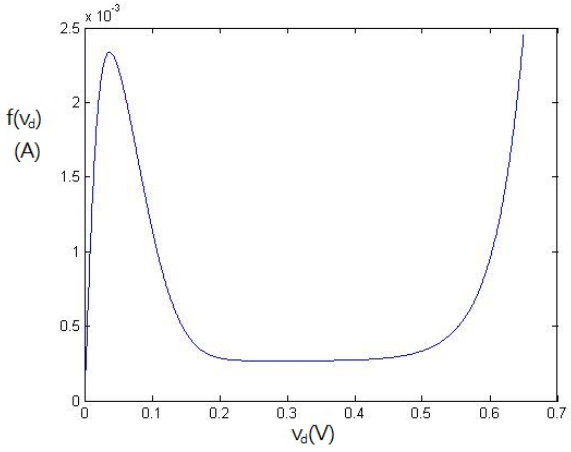

i_1	$-2.2699 \cdot 10^{-3}$ A
C	.1177273
K_1	146.21866 V^{-2}
v_1	$-1.939539 \cdot 10^{-2}$ V
v_2	$1.983499 \cdot 10^{-2}$ V
i_2	$5.985576 \cdot 10^{-10}$ A
v_3	$4.821563 \cdot 10^{-2}$ V

Figure 1: The I-V characteristic curve used in the 3D model. The chart on the right shows the variables used in (1).

When we want to incorporate the tunnel diode into a device or even just measure its current voltage characteristics, some circuit model is implied.

Here for the purpose of matching results we are using a model set up by S.J. Jones in his research. The whole system includes a voltage supply, resistance and capacitance of the power supply, and internal parasitic elements such as the inductance of a thin gold bonding wire that attaches the tunnel diode to its package. The circuit schematic is shown in Figure 2 below.

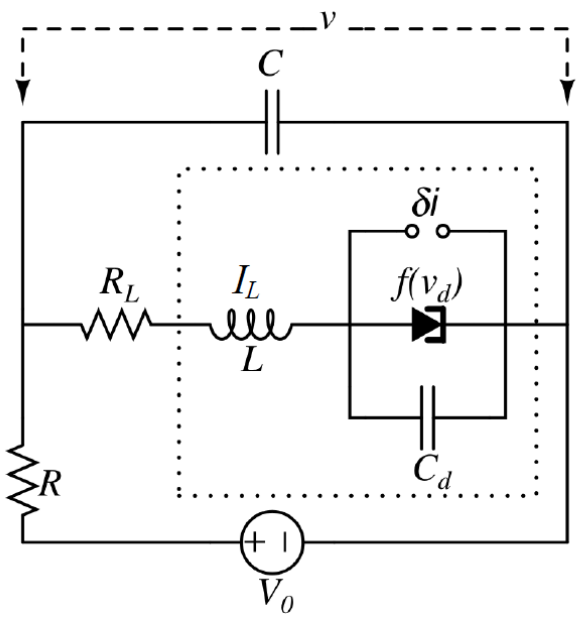

R	22.4 Ω
C	1 nF
L	2 nH
C_d	8 pF
R_L	1 Ω - 100 Ω

Figure 2: This is an equivalent schematic for the tunnel diode measurement circuit described in Ref.[2] The chart on the right gives the parameters of the system.

While noise can play a significant role in the behavior of systems such as the one considered here [6], we will ignore it for the purposes of this paper. Given the circuit implied by the schematic and application of Kirchoff's Laws, we can obtain the following system of equations:

$$\begin{cases} \dot{I_L} = \frac{1}{L}(v - v_d - I_L R_L) \\ \dot{v_d} = \frac{1}{C_d}(I_L - f(v_d)) \\ \dot{v} = \frac{1}{C}((V_0 - v)/R - I_L) \end{cases} \tag{2}$$

This is a nonlinear system that can be described as $\dot{\mathbf{x}} = F(\mathbf{x}, \alpha)$ where $\alpha = [V_0, R_L, R, C, C_d, L]$ and $\mathbf{x} = (I_L, v_d, v)$. Here we are treating V_0 and R_L as bifurcation parameters and the rest are fixed constants for the purpose of studying the 3D model. However, below in the study of a related 2D model some of these parameter will be varied.

By adjusting the bifurcation parameters in the physical system, we are able to observe various bifurcation phenomena. With a high $R_L = 81.6\Omega$ we can observe a hysteresis behavior, which indicates a saddle node bifurcation. While for a lower $R_L = 17.8\Omega$ we instead observe a stable oscillatory behavior. This indicates the existence of a limit cycle, which we can qualitatively take as proof of the existence of Hopf bifurcation.

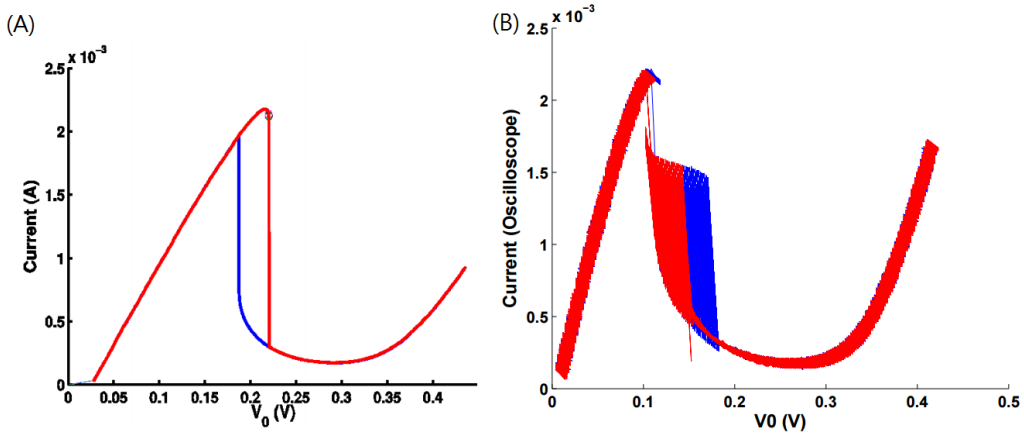

Figure 3: Bifurcation phenomena observed from Steve Jones' thesis [2]. (A) is taken at $R_L = 81.6\Omega$ where a saddle node bifurcation is observed. (B) is taken at $R_L = 17.8\Omega$ where a Hopf bifurcation appears.

One thing worth noting is that if we pick certain R_L in between the occurrence of a Hopf and saddle node bifurcation, we sometimes are able to observe an intermediate behavior as shown in Figure 4. There is clear hysteresis as expected for saddle-node bifurcations, but also intermediate amplitude oscillations, suggestive of Hopf bifurcation. We suspect this behavior indicates the presence of a codimension 2 bifurcation. This will be further discussed in later part of this thesis.

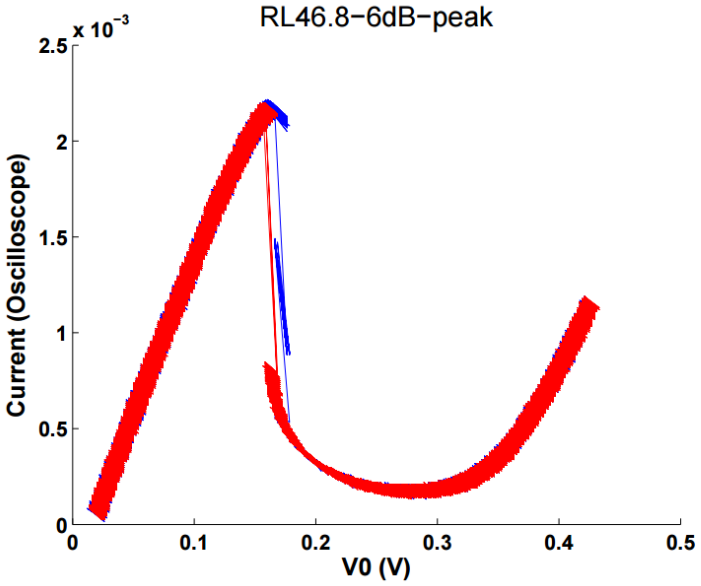

Figure 4: Intermediate bifurcation phenomenon observed from Steve Jones' thesis [2]. Taken at $R_L = 46.8\Omega$ we can see there is a clear hysteresis behavior as well as a limit cycle occur in the blue region .

4 Fixed Point Analysis for 3D system

In order to determine the fixed points, we need to solve $0 = F(\mathbf{x}, \alpha)$. Simple algebra results in the following fixed point condition :

$$f(v_d^*) = \frac{V_0 - v_d^*}{R + R_L} \tag{3}$$

With equations 2 and 3, we can solve for the voltage v_d^* and current $f(v_d^*)$ under different V_0 and R_L. Under this equation, we can also visualize the solution being a single or multiple fixed point based on different V_0 and/or R_L in Figure 5.

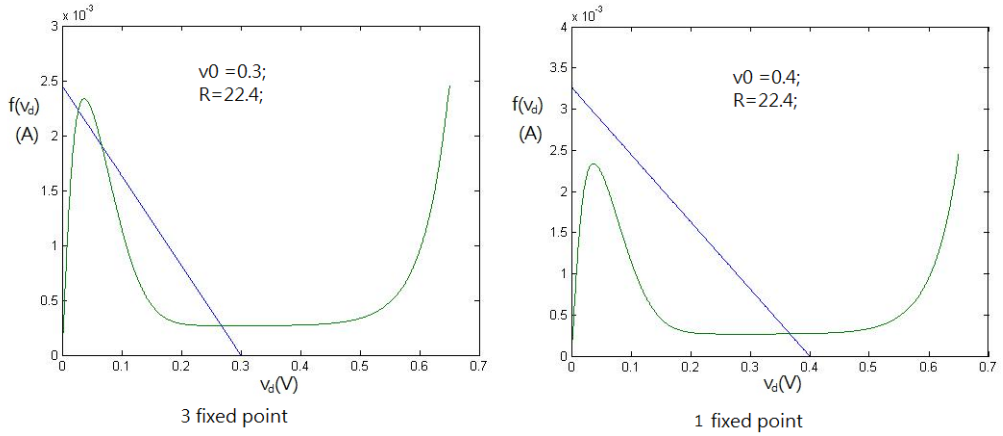

Figure 5: For different V_0, the visualization of different fixed point arrangements.

We can also determine the stability of the fixed points by analyzing the Jacobian of the system. The Jacobian is:

$$J_{FP} = \begin{pmatrix} -\frac{R_L}{L} & -\frac{1}{L} & \frac{1}{L} \\ \frac{1}{C_d} & -\frac{f'(v_d)}{C_d} & 0 \\ -\frac{1}{C} & 0 & -\frac{1}{RC} \end{pmatrix} \tag{4}$$

The number of fixed points and the stability of each fixed point have the potential to change based on changes to V_0 and R_L. We can describe the stability with the following figure.

In Figure 6, region C,D,E contains 3 fixed points two of which are stable and one is unstable (saddle node bifurcation). Outside these regions, there is only one fixed point. Region A contains a stable fixed node. Region B and G have stable spirals, and region F contains an unstable spiral (Hopf

bifurcation). Regions E and H are where the limit cycles appears. The area E (saddle and spiral) is an indication of codimension 2 bifurcation behavior. The MATLAB program for computing this figure is shown in Appendix A.

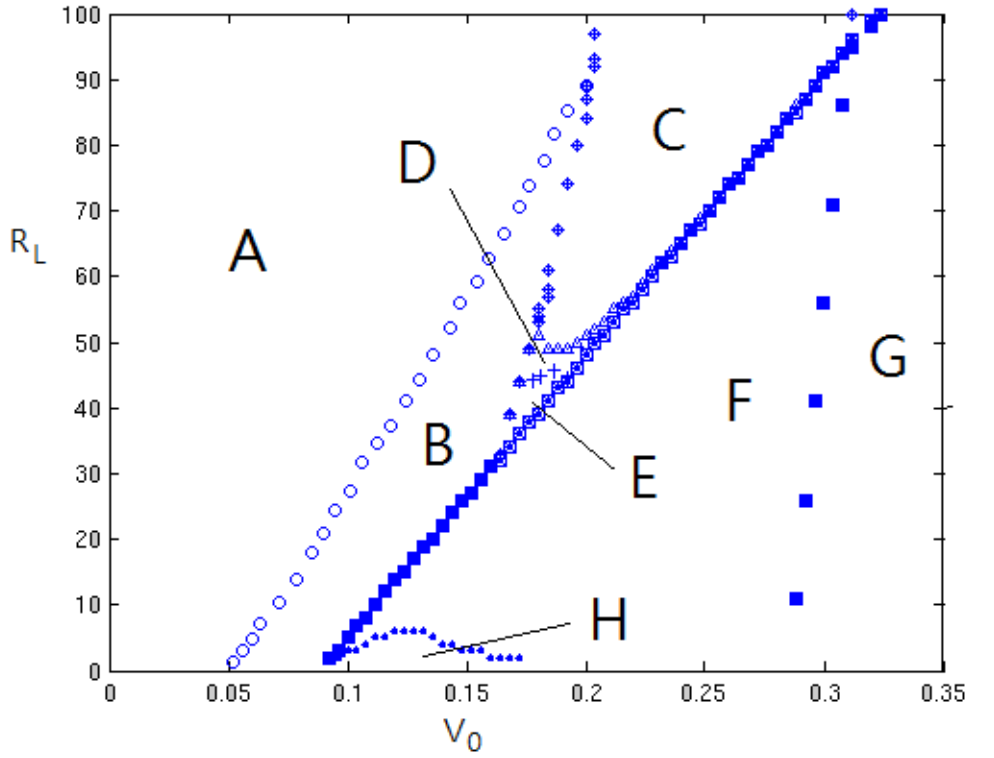

Figure 6: Under different V_0 and R_L, the stability of different fixed points. We divided them into these 8 regions.

5 Cubic approximation of the Tunnel Diode

Despite the fact that we are able to characterize the bifurcation behav-

ior in every area in the 3D system based on the bifurcation parameters, we run into some obstacles trying to unfold the bifurcation behavior around region D and E due to the complicated form of the system. Instead we look through literature to find a different angle of approaching the problem. In "Symmetry-breaking transitions in networks of nonlinear circuit elements", Martin Heinrich offers a simplification of the tunnel diode model by approximating it's behavior with a cubic form [4]. The main idea behind it is that this cubic form will still be able to capture the important negative I-V characteristic of a tunnel diode where most bifurcation action happens without losing much information while significantly simplifying the simulation process and enabling direct mathematical derivation.

We are able to write the tunnel diode's I-V characteristic in the following form:

$$f(v_d) = A[(v - v_{d0})^3 - \alpha(v - v_{d0})] + I_0 \tag{5}$$

In order to determine the parameters we made a few subjective decisions to determine the parameters of the cubic form. Since we want the cubic form the capture behavior in the negative slope region, the cubic form should have the same maximum slope as the complicated form (equation 1) as well as pass through the center of the negative slope region. We also decide to make the equation pass through the origin too, since all I-V curves should start from the origin. Plugging in these points we are able to obtain the parameters

shown in following chart.

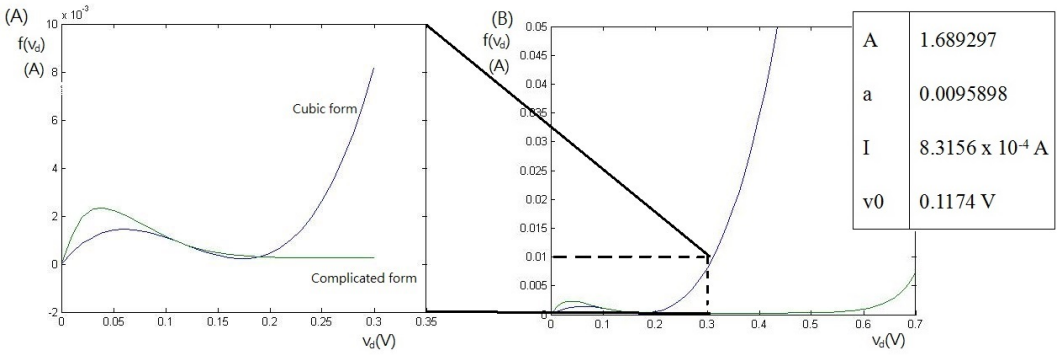

Figure 7: Comparison of cubic form and the complicated form of I-V characteristic. Two figures have different range of V_d, (A) 0-0.3 (B) 0-0.7. The chart on the right are the parameters for the cubic form I-V characteristic.

We are able to compare both the cubic form and the complicated form of the I-V characteristic. As shown in Figure 7, we can see the cubic form (blue) and complicated form(green) perform similarly in the negative slope region as we expected due to the choice of the parameters. The cubic form, however, rises a lost faster than the complicated form. This will lead to an overestimation of the current obtained in the higher voltage region. However this does not affect our purpose of studying the negative slope behavior.

One thing worth noting is that in Martin Heinrich's paper, when he tries to construct the cubic form, he decides to match the local maximum point instead of the center of the negative slope [4]. Both choices accomplish the purpose of capturing the negative slope behavior, but our choice will make the form a lot simpler.

6 2D Simplification of the Tunnel Diode System

We can furthermore simplify the system by removing the capacitance of the power supply in Figure 2. This will give the system shown in Figure 8 and reduce the system to a 2D system.

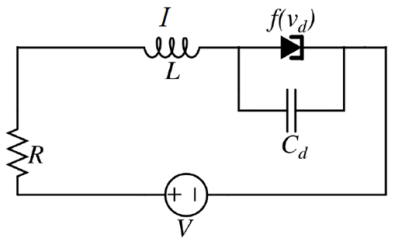

L	10^-7 H
Cd	8*10^-12 F

Figure 8: This is an equivalent schematic for the simplified tunnel diode circuit. The chart on the right gives the parameters of the system.

We are renaming the variable such as I_L and V_0 from Figure 2 to a simpler version as shown in Figure 8. This is to avoid confusion and repetitiveness throughout the rest of the thesis. Given the circuit implied by the schematic and application of Kirchhoff's Laws, we obtain the following:

$$\begin{cases} \dot{I_L} = \frac{1}{L}(V - v_d - IR) \\ \dot{v_d} = \frac{1}{C_d}(I - f(v_d)) \end{cases} \tag{6}$$

The equation $\dot{v}$ that is being eliminated is the fast variable that didn't have much effect on the observe dynamics. We suspect that the simplified

system might still preserve the similar bifurcation phenomena as the 3D system.

7 Non-dimensionalization

Non-dimensionalization is a process to remove units from an equation involving physical quantities by a suitable change of both dependent and independent variables. It simplifies the structure of the system and reduces the changes of dependent variables to order of 1.

In order to further analyze our system of differential equations, we applied non-dimensionalization in order to avoid possible confusion. Since the inductance and capacitance we are working with are extremely small, this process allows us to recover the characteristics of the system and remove possible error caused by units.

Since our cubic form is built around the center point of the negative slope, we decide to use the voltage ($v_{d0} = 1.2 * 10^{-4}$) and current value($I_0 = 8.3 * 10^{-4}$) as the intrinsic reference quantity of the system. For the time variable, we solve for the eigenvalues, L/R and $Cd/f'(v_d)$, from the differential equations. We consulted Martin Heinrich's paper and decided to pick the shorter time as the time reference quantity for convention purposes.

By setting $v_d := v_{d0}x$ and $I := I_0 y$, we are able to obtain the non-dimensionalized system of equations as follows:

$$\begin{cases} \dot{x} = \frac{L}{C_d v_{d0} R}(I_0 y - F(x)) \\ \dot{y} = -\frac{v_{d0}}{I_0 R} x - y + \frac{V}{I_0 R} \end{cases} \tag{7}$$

where $F(x) = f(v_{d0}x)$. We will be referring to this as the system of equations for the rest of the thesis.

8 Theoretical Analysis of the 2D System

Since now we are working on a 2D system as well as a cubic form of the I-V characteristic, we are capable of attempting to derive the bifurcation behavior mathematically.

Saddle node bifurcation occurs when the fixed point condition yeild multiple intersection points with the I-V characteristic. This indicates multiple fixed points, which we treat as sufficient evidence of saddle node bifurcation. For a 2D system, the fixed point condition is identical to Equations 3. We have:

$$f(v_d^*) = \frac{V - v_d^*}{R} \tag{8}$$

By solving for intersection we can obtain the condition for a saddle node bifurcation to occur.

$$R^{SN} > \frac{1}{\alpha A} \tag{9}$$

We can also obtain the same result by solving for the eigenvalues of the system. A saddle node bifurcation occurs when both eigenvalues only have real parts and one of them passes through zero. Using this condition we can obtain the following relationship:

$$R^{SN} = -\frac{1}{f'(v_d)} = \frac{1}{\alpha A - 3A(v_d - v_0)^2}. \tag{10}$$

For Hopf bifurcation to occur, we have eigenvalues as complex conjugate pairs and the real parts going to zero. This gives us the following condition:

$$R^{HB} = -\frac{L}{C_d} f'(v_d) = \frac{L}{C_d}(\alpha A - 3A(v_d - v_0)^2). \tag{11}$$

Similar to Equation 9 and 10 we can rewrite equation 11 into an inequality:

$$R^{HB} < \frac{L}{C_d}\alpha A. \tag{12}$$

For interesting codimension 2 bifurcation to occur, we want the Hopf boundary to be higher than the saddle node boundary. This is $R^{HB}_{max} \geq R^{SN}_{max}$. We get the following condition for codimension 2 bifurcation to occur.

$$\frac{C_d}{L} \leq (\alpha A)^2 \tag{13}$$

For the rest of the thesis we are going to make inductance of the system a changeable parameter. This will enable us to see different behavior between whether the codimension 2 bifurcation appears or not. The critical value for codimension 2 bifurcation to occur is $L \geq 3.0483 * 10^{-8} H$

Due to the fact that a boundary condition exists for saddle node bifurcation (equation 10) and Hopf bifurcation (equation 11) they are both represented with variable v_d. However, v_d is not adjustable throughout the system, it's a reactive variable based on the system setup. We want to represent v_d with V instead.

For saddle node bifurcation, We can expand R close to the minimum bifurcation point $R_*^{SN} = \frac{1}{\alpha A}$. We can obtain the following relationship for the SN boundary in the phase diagram near the minimum value:

$$V - V_*^{SN} = \pm \frac{\alpha^{0.5}}{3\sqrt{3}} \delta R^{1.5} \tag{14}$$

Similarly we can also obtain the form of the Hopf boundary for R close to $R_*^{HB} = \frac{L}{C_d} \alpha A$, this will gives us the following formula:

$$V - V_*^{HB} = -[\frac{L}{C_d}(\alpha A)^2 - 1] \sqrt{\frac{C_d}{3AL}} \delta R^{0.5} \tag{15}$$

We can also obtain these relationships by mapping the v_d with V by the fixed point condition (Equation 8). This will gives us Figure 9.

We can observe for Figure 9-B, there exist a circle within the Hopf region that indicates the codimension 2 behavior. This is similar to region E in Fig-

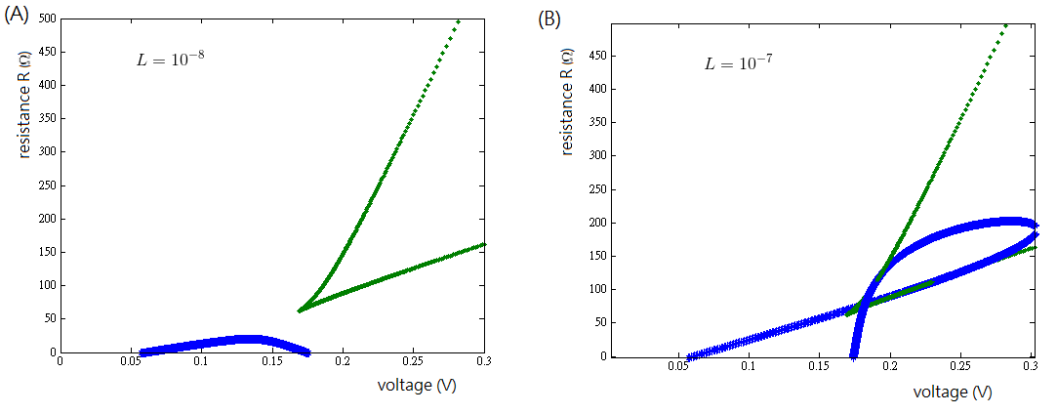

Figure 9: These are theoretical phase diagrams of the 2D system for different inductances. Blue line indicate saddle node bifurcation and Green is for Hopf bifurcation. (A) $L = 10^{-8}$(B) $L = 10^{-7}$

ure 6 of the 3D system. The MATLAB program to calculate the theoretical curve is shown in Appendix B.

9 Numerical Simulation

We then proceed to try unfolding the behavior of bifurcations by doing simulations of the nonlinear ODE's, Equations 7. We decide to construct a "Flow diagram" with the help of Mathmetica. For each system setup (different V and R) we are able to visualize how different initial conditions on the system will evolve until they reach a fixed point or limit cycle.

All of these simulations are under a dimensionless 2D system. Results are shown in the following figures.

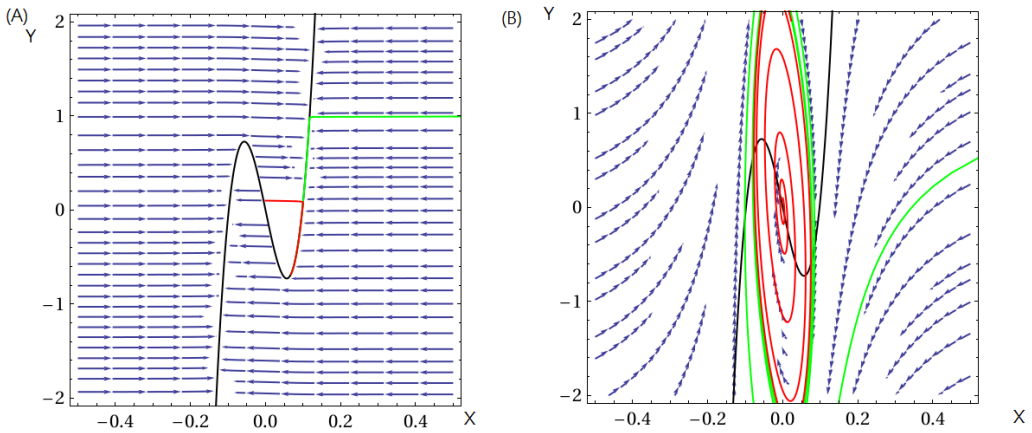

Figure 10: This is the flow diagrams for (A) $V = 0.12V$ and $R = 15\Omega$ (B) $V = 0.24V$ and $R = 150\Omega$. Green and Red line indicates two different trajectory with different initial condition. Black line is the X nullcline.

For Figure 10-A, we can observe a clear saddle node bifurcation. We can see that there are clearly two stable fixed points and no matter where the initial condition is, as long as it's on the same side of the nullcline, it flows to the same fixed point.

For Figure 10-B, we instead observe a limit cycle. This is the evidence of Hopf bifurcation. We can see all the points circle around the unstable fixed point at the center and spiral either in or out to the stable limit cycle based on its initial conditions.

For points inside the Hopf region while within the saddle node bifurcation region, we suspect to have the codimension 2 behavior, which is shown in Figure 11. We can sort of see a spiral around the center, with the saddle node behavior that converge to two different stable fixed points.

All these flow diagrams match the theory derived phase diagram on Figure

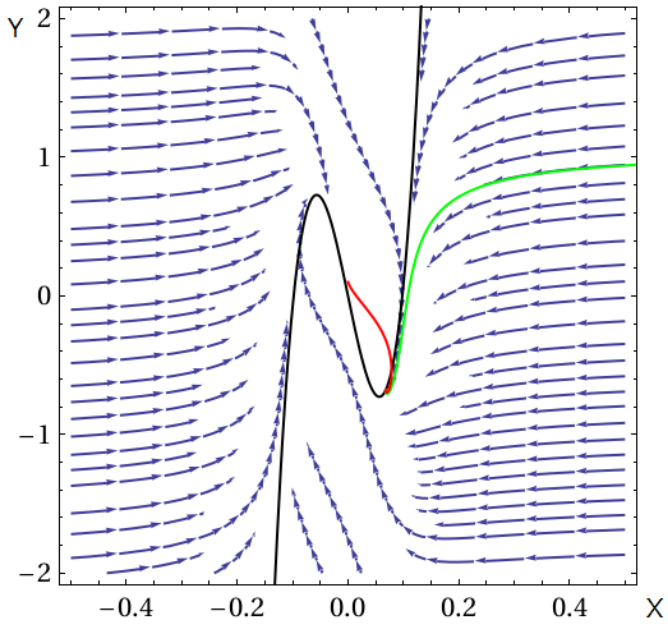

Figure 11: This is the flow diagrams for $V = 0.2V$ and $R = 100\Omega$. Green and Red line indicates two different trajectory with different initial condition. Black line is the X nullcline.

9-B. This provides solid support for the validity of the theory derivation.

We are not able to clearly study the codimension 2 behavior with numerical simulation due to the points mismatch in Mathmetica and Matlab program. We believe this is caused by the rounding we do in the Mathmetica program in order to clear up the format. In the future, we could carry out the numerical simulation in MATLAB. However, there is evidence to supporrt that this is the codimension 2 behavior we are looking at. It shows an interesting spiral performance but acts a lot like saddle node bifurcation. The Mathmatica code to produce these figure is shown in Appendix C.

10 Conclusion Future Goals

In this thesis, we are able to systematically study bifurcation phenomenon in a tunnel diode model. We first study the 3D model that has been experimentally studied by Steve Jones. We are able to successfully construct the circuit model with nonlinear equations, characterize all the bifurcation phenomena by constructing the phase diagram of the system and discover evidence of the codimension 2 bifurcation phenomenon.

We then proceed to simplify the system by replacing the complicated form of I-V characteristic with a cubic form. We also reduce the system to a 2D system. With these simplifications we are able to mathematically derive the bifurcation boundary of the system and determine the conditions for different bifurcations to occur. We also are able to classify the condition for a codimension 2 bifurcation to appear.

We are able to construct a simulation of the system and visualize the behavior of all these bifurcation phenomena. These numerical simulations identify and classify different bifurcations as well as unfolds all the bifurcation phenomena.

However, we still intend to further study the co-dimension 2 bifurcation and unfold its behavior. Are all codimension 2 bifurcation close to saddle node bifurcations? Or is it because the point we chose to conduct simulations with is closer to the saddle node bifurcation region instead. All these

problems will hopefully be solved in the future study.

Also, it may be possible to relate the normal form for our system to results concerning singular Hopf bifurcations that have recently been study by Guckenheimer and co-workers[7-9]. Finally, we note the similarity of our 2D system to the well-studied Fitzhugh-Nagumo model for neuron conduction and the Lienard model for stiff oscillations. [10,11].

11 Reference

1. Okean, H. (1971). Chapter 8 tunnel diodes. In Willardson, R.and Beer, A. C., editors, Applications and Devices Part B, volume 7, Part B of Semiconductors and Semimetals, pages 473

2. Jones, S. J. (2013). A Wide Dynamic Range Tunnel Diode System for Measuring Stochastic Nonlinear Dynamics. Private communication.

3. Jones, S. J. et al. (2012). Tunnel diode global stability analysis. private communication.

4. Heinrich, M. et al.(2010) Symmetry-breaking Transitions in Networks of Nonlinear Circuit Elements. New Journal of Physics 12. DOI: 10.1088/1367-2630/12/11/113030

5. Guter, W. et al. (2006). I-V Characterization of Tunnel Diodes and Multijunction Solar Cells. IEEE Transactions on Electron Devices, volume 53, p.2216-2222. DOI: 10.1109/TED.2006.881051

6. Tretiakov, O. A. et al. (2005). Stochastic current switching in bistable resonant tunneling systems. Phys. Rev. B, 71:165326.

7. Guckenheimer, J. et al. (2012). Unfoldings of singular Hopf bifurcation. SIAM Journal on Applied Dynamical Systems, 11(4):1325–1359. DOI: 10.1137/11083678X

8. Guckenheimer, J. et al. (2012). The Singular Limit of a Hopf Bifurcation. SIAM Journal on Applied Dynamical Systems, 32(8):2805 - 2823,. DOI:10.3934/dcds.2012.32.2805

9. Guckenheimer, J. et al. (2008). Singular Hopf Bifurcation in Systems with Two Slow Variables. SIAM Journal on Applied Dynamical Systems, 7(4):1355–1377. DOI: 10.1137/080718528

10. Izhikevich, E. (2004) Dynamical Systems in Neuroscience: The Geometry of Excitability and Bursting. The MIT Press

11. Strogatz, S. (2000). Nonlinear dynamics and chaos with applications to physics, biology, chemistry, and engineering. Cambridge, MA: Westview Press.

12 Appendix A

Code for generating Figure 6.

```
% the stability analysis
i1=-2.2699*10^-3;
c=0.1177273;
k=146.21866;
v1=-1.939539*10^-2;
v2=1.983499*10^-2;
i2=5.985576*10^-10;
v3=4.821563810^-2;
R=22.4;
C=1*10^-12;
L=2*10^-9;
Cd=8*10^-12;
step = 100;
thresh =0.1;


F=@(x)i1*tanh(x/v1).*(c+exp(-k*(x-v2).^2))+i2.*(exp(x/v3)-1);


dif=@(x)i1*(sech(x/v1)).^2.*(c+exp(-k*(x-v2).^2))/v1-2*i1*exp(-k*(x-v2)
```

```
% stability of the fix point


        counter =1;
 for v0 = 0:0.4/step:0.4
        pt1=0;
        pt2=0;
        pjoc1=0;
        pjoc2=0;
        pval =0;
        pval2=0;
        for RL= 1:100/step:100

        f=@(x)(v0-x)/(R+RL);
        fun=@(x) F(x)-f(x);
        xin = fzero(fun, 0);
        xin1 = fzero(fun,2);
        xin2 = fzero(fun,3);
        delta1= RL/L/Cd/R/C*dif(xin)+dif(xin)/L/c/Cd+1/L/R/C/Cd;
        T1= -RL/L-dif(xin)/Cd-1/R/C;
        joc1=T1.*T1-4*delta1;
        delta2= RL/L/Cd/R/C*dif(xin2)+dif(xin2)/L/c/Cd+1/L/R/C/Cd;
```

```
T2= RL/L-dif(xin2)/Cd-1/R/C;
joc2=T1.*T1-4*delta2;
val =dif(xin);
val2=dif(xin2);

j1 = [-RL/L -1/L 1/L; 1/Cd  -dif(xin)/Cd 0; -1/C 0 -1/R/C];
j2 = [-RL/L -1/L 1/L; 1/Cd  -dif(xin1)/Cd 0; -1/C 0 -1/R/C]
;

if sum(imag(j1))==0;
    if   imag(j1(1))~= 0 | imag(j1(2))~= 0| imag(j1(3))~= 0
        plot(v0,RL,'marker','*','MarkerSize',5);
         hold on;

    end
end

if sum(imag(j2))==0;
    if   imag(j2(1))~= 0 | imag(j1(2))~= 0| imag(j1(3))~= 0
        plot(v0,RL,'marker','-','MarkerSize',5);
         hold on;

    end
```

```
end

    if val.*pval <0;
            plot(v0,RL,'marker','o','MarkerSize',5);
            hold on;
          end
if val2.*pval2 <0;
            plot(v0,RL,'marker','+','MarkerSize',5);
            hold on;
 end

    if T1.*pt1 <0;
         plot(v0,RL,'marker','.','MarkerSize',5);
          hold on;


     end

     if joc1.*pjoc1<0;
         plot(v0,RL,'marker','s','MarkerSize',5);
          hold on;
     end

     if T2.*pt2<0;
```

```
            plot(v0,RL,'marker','d','MarkerSize',5);
            hold on;
        end

        if joc2.*pjoc2<0;
            plot(v0,RL,'marker','^','MarkerSize',5);
            hold on;
        end
    pt1=T1;
    pt2=T2;
    pjoc1=joc1;
    pjoc2=joc2;

     pval = val;
     pval2 = val2;
    end

    counter =counter +1;
end
```

13 Appendix B

Code for generating Figure 9.

```
% theoritical plots
L=10^-7;  % input
%parameter
Cd=8*10^-12;
A=1.689297;
a= 0.0095898;
I = 8.3156*10^-4;
v0 = 0.1174;
F=@(x)A.*((x-v0).^3-  (a.*(x-v0)))+I;

for vd=0:0.0001:0.3

    r1= L/Cd*[a*A-3*A*(vd-v0)^2];
    r2=1/[a*A-3*A*(vd-v0)^2];

    v1=r1*F(vd)+vd;
    v2=r2*F(vd)+vd;
    plot(v1,r1,'*',v2,r2,'.')
    hold on
end
```

14 Appendix C

Code for generating Figure 10 and 11.

```
%flow chart
flowc1 = StreamPlot[{10 (y - 2011 x^3 + 19.305 x), -y -10 x},
{x, -0.5, 0.5}, {y, -2, 2}]


% nullclines
nc0 = Plot[-10 x, {x, -0.5, 0.5}, PlotStyle -> Red]
nc1 = Plot[2011 x^3 - 19.305 x, {x, -0.5, 0.5}, PlotStyle ->
Black]


%simulation
s = NDSolve[{x'[t] == 10 (y[t] - 2011 x[t]^3 + 19.305 x[t]), y'[t]
== -y[t] - 10 x[t], x[0] == 1, y[0] == 1}, {x, y}, {t, 11}]
yc1 = Plot[Evaluate[y[t] /. s], {t, 0, 11}, PlotRange -> All]
xc1 = Plot[Evaluate[x[t] /. s], {t, 0, 11}, PlotRange -> All]
rk1 = ParametricPlot[Evaluate[{x[t], y[t]} /. s], {t, 0, 11},
PlotStyle -> Green, PlotRange -> All]


q = NDSolve[{x'[t] == 10 (y[t] - 2011 x[t]^3 + 19.305 x[t]), y'[t]
== -y[t] - 10 x[t], x[0] == 0, y[0] == 0.1}, {x, y}, {t, 11}]
yc2 = Plot[Evaluate[y[t] /. q], {t, 0, 11}, PlotRange -> All]
```

```
xc2 = Plot[Evaluate[x[t] /. q], {t, 0, 11}, PlotRange -> All]
rk2 = ParametricPlot[Evaluate[{x[t], y[t]} /. q], {t, 0, 11},
PlotStyle -> Red, PlotRange -> All]

%combine
comb1 = Show[flowc1, nc1, rk1, rk2,  PlotRange -> {{-0.5, 0.5},
{-2, 2}}]
```